Control-Oriented Modeling of Electrode Material for Mechanical Notching and Stacking Processes of Battery Manufacturing

Andreas Rauh and Lisa Wünderlich
Group: Distributed Control in Interconnected Systems
Carl von Ossietzky Universität Oldenburg
Oldenburg, Germany
{andreas.rauh, lisa.wuenderlich}@uni-oldenburg.de

***Abstract*—The processes of notching and stacking represent two crucial stages of battery cell manufacturing that have a significant influence on the quality of the produced cells from the perspective of lifetime. In addition, these stages are also crucial concerning safety, especially, when the production of cells with high energy density is concerned. This is due to the fact that imperfect cutting edge quality in notching (due to burr) may lead to sharp edges that cut through separator foils when stacking is executed. This may produce internal short circuits in produced cells that are possibly not detected during the formation stage but only show up during operation when internal pressure and temperature variations in battery cells lead to a gradual extension of this defect. The same is also true for mechanical deformations of electrodes during their transport within the stacking process which may lead to wrinkles as well as cracks. Therefore, this paper presents a control-oriented modeling procedure for flexible electrodes that can be used for forecasting deflections in elastic and plastic regimes during notching and stacking and therefore is inevitable for a model-based design of control strategies for both handling stages. The core of this modeling approach is the replacement of the governing partial differential equation for the material deformation by a model that is discretized in space and time. For that purpose, the Crank–Nicolson approach is employed due to its favorable property of preserving the stability properties when discretizing the underlying infinite-dimensional model.**

***Index Terms*—Battery cell manufacturing, control-oriented modeling, Crank–Nicolson discretization, elastic and plastic deformation of flexible material**

I. Introduction

For the purpose of analyzing manufacturing processes, for their redesign and control optimization, as well as for the early detection of root causes of defective products, the development of digital twins is gaining more and more importance [4], [7]. In all cases, these digital twins help to realize a bi-directional flow of information. On the one hand, information is gathered from the process to be observed. On the other hand, the digital twins are employed to feed back information so that manufacturing or use of the components is enhanced or that novel functionalities (such as life-time monitoring) can be achieved. The latter, for example, can turn passive components into actual cyber-physical systems.

Concerning this bi-directional flow of information, different levels of digital twins can be distinguished if manufacturing processes are concerned [4]:

- System-level digital twins aiming at an enhancement of supervisory control strategies within a factory, mostly in the frame of tracking the flow of material;
- Process-level digital twins, representing the actual physical cause-effect relationships in the individual production stages, which are employed for offline optimization, production monitoring, and online state estimation as well as disturbance compensation;
- Product-level digital twins associating specific product properties to selected manufacturing stages, including the implementation of digital product passports that monitor not only functional properties but also extra-functional ones such as the consumption of energy and raw material during production and the associated ecological footprint due to emissions.

In this paper, we consider two selected mechanical production stages within the manufacturing of battery cells [6], namely, the stages of notching and stacking [9]. Firstly, in notching a mechanical (plastic) deformation of material takes place due to the cutting of the electrode foils into their final shape, where the material has already been coated with active material, calendered, and dried in previous stages. Secondly, the individual electrodes are stacked with separator foils in between during the following downstream manufacturing stage. Here, especially, elastic deformation takes places during the movement of material. Moreover, damage of separator and electrode material needs to be prevented both by a reduction of burr in the cutting phase and by keeping material deformation during stacking within pre-defined tolerance bounds.

To solve these aforementioned tasks, it is essential to derive a mathematical material model that can be exploited for the design and implementation of control approaches in both manufacturing stages. For that purpose, we propose an approach that discretizes the underlying partial differential

This project has received funding from the European Union's Horizon Europe programme under grant agreement No. 101137954. The authors would like to thank the rest of the BATTwin consortium for supporting this research.

equation (PDE) of a thin flexible sheet of material with the help of the Crank–Nicolson method [5]. This approach, leading to a full discretization in space and time, has already been exploited for other tasks, in which the deformation of deformable material was purposefully controlled [1]–[3]. In contrast to other discretization methods, it has the advantage of preservation of stability properties. In addition to the task of modeling, this paper formulates the model explicitly in such a way that it can be used for further tasks of control and state estimator design. In such a way, the proposed modeling approach represents a fundamental component of the development of a comprehensive digital twin platform for battery manufacturing within the Horizon Europe project BATTWIN[1], where physics-based models form the basis for the development of the above-mentioned digital twins on process level.

This paper is structured as follows. Sec. II summarizes modeling of the mechanical behavior of a flexible electrode by means of a Crank–Nicolson discretization scheme. This model is further detailed for the process of notching in Sec. III together with a numerical simulation case study that allows for a quantification of the appearance of burr. Analogously, the transport of electrodes during stacking is taken into consideration in Sec. IV, before the paper is concluded with an outlook on future work in Sec. V.

II. Crank–Nicolson Discretization of Flexible Electrode Material

A. Spatially Distributed PDE Model of the Electrode Deflection

Throughout this paper, we consider a membrane-like electrode model represented by the fourth-order PDE [1], [2], [8]

$$\frac{\partial^4 w}{\partial x^4} + 2\frac{\partial^4 w}{\partial x^2 \partial y^2} + \frac{\partial^4 w}{\partial y^4} + \frac{\rho}{D}\frac{\partial^2 w}{\partial t^2} = \frac{f(t,x,y)}{D} \tag{1}$$

of Lagrangian type. This model represents the deflection $w := w(t,x,y)$ out of the (x,y)-plane — representing the electrode in its mechanically energy-free equilibrium state — under the influence of the external, spatially distributed force $f(t,x,y)$ per unit area. In (1), ρ is the mass per unit area and

$$D = \frac{Eh^3}{12\left(1-\nu^2\right)} \tag{2}$$

is expressed in terms of the membrane thickness h, the Poisson ratio ν, and Young's modulus E. The membrane is assumed to have the dimensions $x \in [0\,;\,L_{\mathrm{x}}]$ and $y \in [0\,;\,L_{\mathrm{y}}]$ with $h \ll L_{\mathrm{x}}$ and $h \ll L_{\mathrm{y}}$. To make the model valid for forecasting the deflection of an electrode during notching and stacking, we assume further that the compound material (foil with the electrochemically active coating) is treated as a homogeneous membrane, where ν and E represent averaged material properties.

To account for viscous (velocity-proportional) and nonlinear damping as well as for restoring spring forces (proportional to the deflection w) and plastic deformation effects, the two additional, spatially varying forces

$$f_{\mathrm{d}}(t,x,y) = f_{\mathrm{d}}\left(\frac{\partial w(t,x,y)}{\partial t}\right) \tag{3}$$

and

$$f_{\mathrm{s}}(t,x,y) = f_{\mathrm{s}}\left(w(t,x,y)\right) \quad , \tag{4}$$

respectively, are introduced.

This leads to an extension of the model (1) in the form

$$\begin{aligned}&\frac{\partial^4 w}{\partial x^4} + 2\frac{\partial^4 w}{\partial x^2 \partial y^2} + \frac{\partial^4 w}{\partial y^4} + \frac{\rho}{D}\frac{\partial^2 w}{\partial t^2} = \\ &\qquad \frac{f(t,x,y) - f_{\mathrm{d}}(t,x,y) + f_{\mathrm{s}}(t,x,y)}{D} = \frac{\tilde{f}(t,x,y)}{D} \quad .\end{aligned} \tag{5}$$

B. Second-Order Centralized Discretization Using the Crank–Nicolson Scheme

An approximation of the infinite-dimensional model (5) by a representation that is discretized in both space and time makes it applicable for simulation and, for example, control design. For this, we exploit a second-order Crank–Nicolson scheme [5] that represents the deflection w in the form $w_{k,i,j}$ at discrete points in time k for selected spatial discretization points denoted by the indices (i,j). For that purpose, we assume an equidistant spatial discretization mesh (x_i, y_j), $i \in \{0,\ldots,N_{\mathrm{x}}\}$, $j \in \{0,\ldots,N_{\mathrm{y}}\}$ with

$$\Delta x = x_{i+1} - x_i = \frac{L_{\mathrm{x}}}{N_{\mathrm{x}}} \tag{6}$$

and

$$\Delta y = y_{j+1} - y_j = \frac{L_{\mathrm{y}}}{N_{\mathrm{y}}} \quad . \tag{7}$$

In the time domain, the discretization step size is set to the constant $\Delta T = t_{k+1} - t_k$.

This discretization, as discussed in detail in [1]–[3], [5], approximates the velocity field in the form

$$\frac{\partial w}{\partial t} \approx \dot{w}_{k,i,j} = \frac{w_{k+2,i,j} - w_{k,i,j}}{2\Delta T} \tag{8}$$

and the respective acceleration by

$$\frac{\partial^2 w}{\partial t^2} \approx \ddot{w}_{k,i,j} = \frac{w_{k+2,i,j} - 2w_{k+1,i,j} + w_{k,i,j}}{\Delta T^2} \quad . \tag{9}$$

The spatial derivatives are analogously approximated by

$$\frac{\partial^4 w}{\partial x^4} \approx \frac{w_x^{(4)}(k+2) + 2w_x^{(4)}(k+1) + w_x^{(4)}(k)}{4} \tag{10}$$

with

$$\begin{aligned}w_x^{(4)}(k) = \frac{1}{4\Delta x^4}\cdot\big(&w_{k,i-2,j} - 4w_{k,i-1,j} + 6w_{k,i,j} \\ &-4w_{k,i+1,j} + w_{k,i+2,j}\big) \quad ,\end{aligned} \tag{11}$$

$$\frac{\partial^4 w}{\partial y^4} \approx \frac{w_y^{(4)}(k+2) + 2w_y^{(4)}(k+1) + w_y^{(4)}(k)}{4} \tag{12}$$

with

$$\begin{aligned}w_y^{(4)}(k) = \frac{1}{4\Delta y^4}\cdot\big(&w_{k,i,j-2} - 4w_{k,i,j-1} + 6w_{k,i,j} \\ &-4w_{k,i,j+1} + w_{k,i,j+2}\big) \quad ,\end{aligned} \tag{13}$$

[1] www.battwin.eu

and

$$\frac{\partial^4 w}{\partial x^2 \partial y^2} \approx \frac{w_{xy}^{(4)}(k+2) + 2w_{xy}^{(4)}(k+1) + w_{xy}^{(4)}(k)}{4} \tag{14}$$

with

$$\begin{aligned} w_{xy}^{(4)}(k) =& \frac{1}{4\Delta x^2 \Delta y^2} \cdot (w_{k,i-1,j-1} - 2w_{k,i-1,j} + w_{k,i-1,j+1} \\ & - 2w_{k,i,j-1} + 4w_{k,i,j} - 2w_{k,i,j+1} \\ & + w_{k,i+1,j-1} - 2w_{k,i+1,j} + w_{k,i+1,j+1}) \quad . \end{aligned} \tag{15}$$

In addition, we discretize the second- and third-order space derivatives (that are required in the following for expressing boundary conditions at the edges of the electrode) in the form

$$w_x^{(2)}(k) = \frac{1}{\Delta x^2} \cdot (w_{k,i-1,j} - 2w_{k,i,j} + w_{k,i+1,j}) \tag{16}$$

and

$$\begin{aligned} w_x^{(3)}(k) = \frac{1}{2\Delta x^3} \cdot (&-w_{k,i-2,j} + 2w_{k,i-1,j} \\ &-2w_{k,i+1,j} + w_{k,i+2,j}) \end{aligned} \tag{17}$$

for derivatives in x-direction and by

$$w_y^{(2)}(k) = \frac{1}{\Delta y^2} \cdot (w_{k,i,j-1} - 2w_{k,i,j} + w_{k,i,j+1}) \tag{18}$$

and

$$\begin{aligned} w_y^{(3)}(k) = \frac{1}{2\Delta y^3} \cdot (&-w_{k,i,j-2} + 2w_{k,i,j-1} \\ &-2w_{k,i,j+1} + w_{k,i,j+2}) \end{aligned} \tag{19}$$

for the ones in y-direction.

C. Boundary Conditions

This subsection gives an overview of all boundary conditions at the edges of the processed material that are necessary subsequently for modeling notching and stacking.

1) Clamped Edge of the Electrode: During cutting processes, typically at least one of the edges of an electrode is clamped to the cutting table. Assume that the corresponding index set of edge elements is given by the index tuples $\{i_{\mathrm{cl}}, y_{\mathrm{cl}}\}$ listed in the set

$$\mathcal{I}_{\mathrm{cl}} = (\{i_{\mathrm{cl}}, y_{\mathrm{cl}}\}) \quad . \tag{20}$$

The respective boundary conditions are then

$$w_{k,i,j} = w_{\mathrm{cl}} \quad \text{with} \tag{21}$$

$$\dot{w}_{k,i,j} = 0 \quad \text{and} \quad \ddot{w}_{k,i,j} = 0 \tag{22}$$

for all $(i,j) \in \mathcal{I}_{\mathrm{cl}}$ and all $k \in \mathbb{N}_0$.

2) Free Boundary Condition: For free edges of the electrode, boundary conditions need to be introduced that ensure that neither bending torques nor shear forces act on the electrode edges. This is achieved by setting the respective second- and third-order spatial derivatives at the free boundaries in Eqs. (16), (17) and/or Eqs. (18), (19) to zero for all $k \in \mathbb{N}_0$. This ensures that also the time derivatives of all of these boundary conditions remain zero for all points in time.

3) Line Force at an Edge of the Electrode: To account for force inputs at a selected edge of the electrode, the second-order space derivative approximations (16) or (18) are set to zero (where the choice depends on whether it is an edge on the x or y boundaries). In addition, the respective expressions (17) or (19) are set equal to the corresponding force that depends either on the electrode deflection $w_{k,i,j}$ at the boundary (restoring force representing a material spring-back effect) or on the time index k (model of an open-loop control force).

4) Elimination of Deflections Specified by Boundary Conditions: As it can be seen in the approximations (10)–(15), the discretized representation of the PDE (5) depends not only on displacements $w_{k,i,j}$ at interior and edge nodes characterized by all combinations of indices $i \in \{0, \ldots, N_{\mathrm{x}}\}$ and $j \in \{0, \ldots, N_{\mathrm{y}}\}$ but also on indices taking on values from the ranges $i \in \{-2, 1, N_{\mathrm{x}}+1, N_{\mathrm{x}}+2\}$ and $j \in \{-2, 1, N_{\mathrm{y}}+1, N_{\mathrm{y}}+2\}$.

These values are eliminated by accounting for the expressions mentioned in the Subsections II-C1, II-C2, and II-C3.

After this elimination, the system model (5) is replaced by the implicit discrete-time system model

$$\tilde{\mathbf{F}}(\mathbf{w}_k, \mathbf{w}_{k+1}, \mathbf{w}_{k+2}) = \mathbf{0} \quad . \tag{23}$$

A discrete-time state-space representation

$$\mathbb{W}_{k+1} = \mathbf{f}(\mathbb{W}_k, \mathbb{U}_k) \tag{24}$$

is then finally obtained if the state vector (summarizing discrete-time deflection values at the points k and $k+1$) according to

$$\mathbb{W}_k = \begin{bmatrix} \mathbf{w}_k^T & \mathbf{w}_{k+1}^T \end{bmatrix}^T \tag{25}$$

is introduced. Here, the index set (i,j) of the vectors $\mathbf{w}_k$ and $\mathbf{w}_{k+1}$ summarizing the deflections $w_{k,i,j}$ and $w_{k+1,i,j}$, respectively, does not contain values outside the index ranges $i \in \{0, \ldots, N_{\mathrm{x}}\}$ and $j \in \{0, \ldots, N_{\mathrm{y}}\}$ as those have been eliminated before. Moreover, also all deflection values are eliminated that are predefined due to clamped edges.

In addition, the vector $\mathbb{U}_k$ contains the discrete-time external control inputs $u_{k,i,j}$ at the coordinates (x_i, y_j) that are directly influenced by the purely time-dependent line force mentioned above or by a force $f(t,x,y)$ introduced by means of an actuator over the material surface (cf. eqs. (1) and (5)).

An example for such kind of force is presented in Section IV, where the actuation of a gripper is determined with heuristically tuned PD- and PID-type control laws.

Remark 1: The resolution of the model (23) is possible in closed form, if the force boundary conditions according to Subsection II-C3 do not contain nonlinear terms in $\mathbf{w}_{k+2}$. This is either guaranteed if only linear force models are accounted for or if terms that are nonlinear in $\mathbf{w}_{k+2}$ are approximated prior to the reformulation into an explicit set of state equations.

Remark 2: The approximation according to the previous remark can be avoided if these nonlinear forces are *not* formulated in terms of boundary conditions but if they are instead included in the right-hand side of (5) within $f(t,x,y)$ or in the terms $f_\mathrm{d}(t,x,y)$ and $f_\mathrm{s}(t,x,y)$ defined in (3) and (4).

Remark 3: The state-space representation (24) typically has a dominating linear behavior for deflections $w_{k,i,j}$ that do not vary by a large extent over the complete electrode surface. Therefore, future research for optimizing state-feedback control approaches can make use of polytopic uncertainty representations for a quasi-linear formulation of (24), allowing for controller tuning with the help of linear matrix inequality techniques. This holds similarly if iterative learning control procedures similar to those in [1]–[3] are designed that aim at enhancing the control performance from one execution of the notching (resp., stacking) task to the next.

III. Notching

In this section, we focus on a first demonstration scenario in which plastic deformation of the electrode material at the cutting edge during a mechanical notching process is taken into consideration. A spring-back behavior starts at the point in time where the cutting is finished and leads to a steady-state deformation of the material due to plastic deformation. The resulting magnitude of deformation allows for a quantification of the occurrence of burr in a probabilistic manner.

For that purpose, we assume that three edges of the electrode are rigidly clamped and that one edge (the one at which cutting takes place) is initially deflected and subject to a nonlinear restoring force. The initial deflection represents the electrode position at the end of cutting, while the nonlinear force is a phenomenological representation of plastic deformation.

Without loss of generality concerning the presentation of this modeling approach, we neglect gravitational effects and nonlinear forces in the interior of the material. This means that apart from the cutting edge, only linear spring forces and oscillation attenuation are taken into consideration.

A. Phenomenological Model of Plastic Deformation of the Cutting Edge

Firstly, consider a straight-line cut at the edge $i = N_\mathrm{x}$, $j \in \{1,\ldots,N_\mathrm{y}\}$, $(i,j) \in \mathcal{I}_\mathrm{cut}$. Under the assumptions described above, we include the force

$$\begin{aligned} f_{\mathrm{s},k,i,j} = &-k_1 w_{k,i,j} - k_2 \mathrm{sign}\left(w_{k,i,j}\right) \\ &- k_1 w_{k+1,i,j} - k_2 \mathrm{sign}\left(w_{k+1,i,j}\right) \end{aligned} \tag{26}$$

that is acting at the cutting edge onto the electrode in addition to the forces introduced in Eq. (5). For the straight-line cutting, it is included in the form of the boundary condition described in Sec. II-C3. Moreover, the velocity-proportional damping force is given by $f_\mathrm{d} = k_\mathrm{d} \cdot \dot{w}$ according to Eq. (3). The initial deflection at the cutting edge is set to

$$w_{0,N_\mathrm{x},j} = -0.6 \sin\left(\frac{\pi y_j}{L_\mathrm{y}}\right) \quad \text{and} \quad w_{1,N_\mathrm{x},j} = -0.6 \sin\left(\frac{\pi y_j}{L_\mathrm{y}}\right) \tag{27}$$

at the index set $(i,j) \in \mathcal{I}_\mathrm{cut}$ listed above.

Second, more complex cutting geometries can be easily accounted for by specifying a polygonal contour in the index set $\mathcal{I}_\mathrm{cut}$. An example is depicted graphically in Sec. III-B. Here, the force $f_{\mathrm{s},k,i,j}$ is introduced according to Remark 2. To obtain an approximately equal scaling, it is multiplied with the factor $D \cdot \frac{1}{8\Delta y^3}$.

B. Analysis of the Spring-Back Behavior at the Cut Material Edge and Quantification of the Severity of Burr

For the analysis of the spring-back effect, consider the parameter values listed in Tab. I. Here, the value r is a uniformly distributed random value chosen independently for each node on the cutting line from the interval $[0\ ;\ 1]$ to reflect a random plastic deformation in a phenomenological manner. For a real material, this value needs to be calibrated such that the true deformation along the cutting line in steady-state represents the actual behavior (step size $\Delta T = 0.01$).

TABLE I: Parameters of the notching model (normalized to SI units).

par.	L_x	L_y	N_x	N_y	$\frac{\rho}{D}$	$\frac{k_\mathrm{d}}{D}$	$\frac{\rho g}{D}$	k_1	k_2
value	3	1.5	30	15	2	5	$2 \cdot 9.81$	0.1	$0.1r$

Fig. 1 shows the steady-state deformation of the electrode after a single execution of the notching task. Repeating the corresponding simulation, with an identical initial deflection profile, however, disturbed with a standard deviation of 0.01 and new random values for the parameter r leads to different steady-state deflections. These steady-state profiles represent a measure for the occurring burr at the cutting edge. Its severity is quantified by means of the frequency plot shown in Fig. 2.

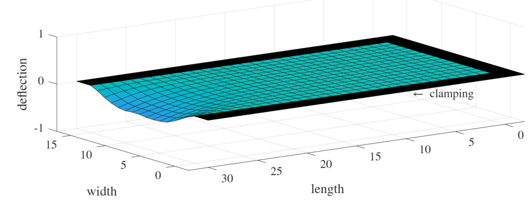

Fig. 1: Steady-state for a straight-line cut, positions are indicated by the indices (i,j).

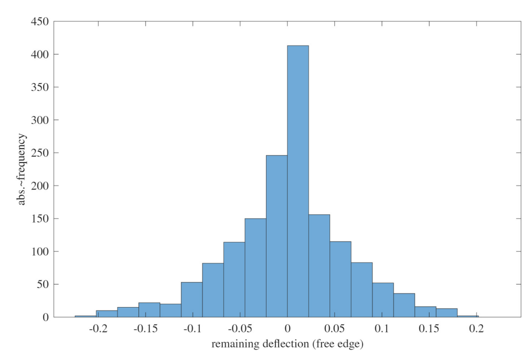

Fig. 2: Frequency distribution of burr (straight-line cut) for 100 repetitions of the notching process.

Figs. 3 and 4 correspond to a repetition of the simulation including the quantification of the severity of burr if the nonlinear material force is not introduced as a boundary force but rather as an external line force on the surface as described in Remark 2. In addition, it is shown that the proposed simulation method allows also to characterize the steady-state deflection despite a polygonal cutting geometry.

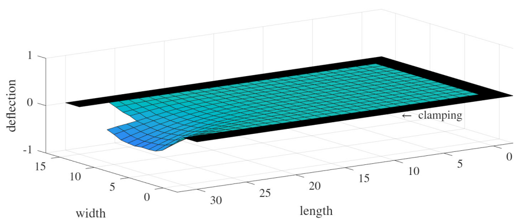

Fig. 3: Steady-state deflection for polygonal cutting line.

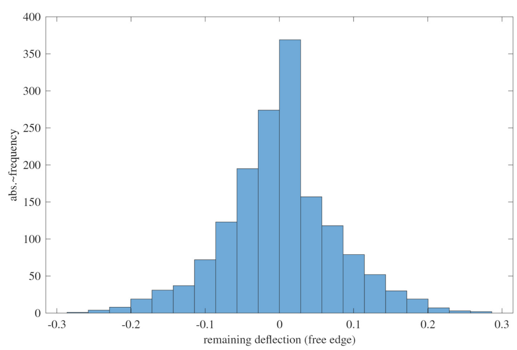

Fig. 4: Frequency distribution of burr (polygonal cutting line) for 100 repetitions of the notching process.

IV. Stacking

The second demonstration scenario in this paper is concerned with the elastic deformation of the electrode during the transportation phases of stacking. For that purpose, the actuating force of a handling system is applied in four equally large, rectangular gripping areas of the electrode which are placed in a symmetric manner. The symmetry consists of twice axial symmetric orientation (wrt. the midpoints of each edge) as well as point symmetry wrt. the electrode's center.

A. Coupling of the Material Model with Control Approaches

For control purposes, two different scenarios are considered. These are alternatively the assumption of a homogeneous force over each of the four gripper areas (leading to a deformation of the gripped area due to flexibility of the material) and spatially varying forces (reducing the deformation).

In both cases, we consider a point-to-point motion for the electrode (in the first case wrt. the average gripper position orthogonal to the electrode surface) along a linear desired position profile $w_{\mathrm{d},k}$ during the transport. The controllers are modeled as simple linear output feedback control laws of proportional–differentiating (PD) and proportional–integrating–differentiating (PID) types that act on the electrodes via the discretization nodes $(i,j) \in \mathcal{I}_\mathrm{c}$. Using the notation (24), the force values $f_{\mathrm{c},k,i,j}$ are summarized in the input vector $\mathbb{U}_k$.

In the case of a homogeneous actuator force, a PD controller

$$f_{\mathrm{c},k,i,j} = f_{\mathrm{g},k,i,j} + \frac{1}{4N_\mathrm{c}} \cdot \sum_{(i,j)\in\mathcal{I}_\mathrm{c}} \Big(K_\mathrm{p} \left(w_{\mathrm{d},k} - w_{k,i,j}\right) - \frac{K_\mathrm{d}}{\Delta T}\left(w_{k,i,j} - w_{k-1,i,j}\right)\Big) \ , \quad (i,j) \in \mathcal{I}_\mathrm{c} \tag{28}$$

is employed, while a PID controller

$$f_{\mathrm{c},k,i,j} = f_{\mathrm{g},k,i,j} + K_\mathrm{p}(w_{\mathrm{d},k} - w_{k,i,j}) - \frac{K_\mathrm{d}}{\Delta T}(w_{k,i,j} - w_{k-1,i,j}) + K_\mathrm{i}\sum_{\kappa=0}^{k}\left(w_{\mathrm{d},k} - w_{\kappa,i,j}\right) \ , \quad (i,j) \in \mathcal{I}_\mathrm{c} \tag{29}$$

is used for reducing deflections over the gripper areas for the spatially varying case. In both (28) and (29), the force

$$f_{\mathrm{g},k,i,j} = g\frac{(1+N_\mathrm{x})(1+N_\mathrm{y})}{4N_\mathrm{c}} \tag{30}$$

serves for a compensation of gravitational effects acting homogeneously over the complete electrode surface by the four grippers, each comprising N_c grid points. For all points outside the index set $\mathcal{I}_\mathrm{c}$, the forces $f_{\mathrm{c},k,i,j}$ according to (28) and (29) are zero. Including gravitational effects, the force $f(t,x,y)$ in (5) is then approximated by the spatially and temporally discretized form

$$f_{k,i,j} = f_{\mathrm{c},k,i,j} - g\frac{1}{(1+N_\mathrm{x})(1+N_\mathrm{y})} \ . \tag{31}$$

For the heuristically chosen gains $K_\mathrm{p} = 2.5$ and $K_\mathrm{d} = \Delta T \cdot 0.05$ in (28) and $K_\mathrm{p} = 25$, $K_\mathrm{d} = 0$, and $K_\mathrm{i} = 0.5$ in (29), Figs. 5(a)–5(c) and Figs. 6(a)–6(b) show the deflection of the electrode at various points in time for the transport of the electrode. The reference position of the transport is given by

$$w_{\mathrm{d},k} = \begin{cases} 0 & \text{for} \quad k < 100 \\ 4 \cdot \frac{k-100}{900} & \text{for} \quad 100 \leq k < 1000 \\ 4 & \text{for} \quad k \geq 1000 \ . \end{cases} \tag{32}$$

In all figures in this section, the parameters, including the ones for the velocity-proportional damping are chosen as in Tab. I. However, spring-back phenomena are not considered in the simulations shown in Figs. 5(a)–5(c) and Figs. 6(a)–6(b).

B. Inclusion of Plastic Deformation and Integration with the Notching Stage

As a final case study, nonlinearities are introduced in Fig. 6(c) by a surface force similar to Eq. (26). In contrast to notching, where the steady-state in absence of this nonlinear force would be given by $w = 0$, the nonlinear force model is now based on point-wise deviations of the deflection $w_{k,i,j}$ form the average deflection of the electrode at the same point in time. Moreover, the force is scaled by a factor in the order of magnitude of 10^{-3} in comparison to the notching section, to reflect the property that stacking mostly only excites elastic deformation. A comparison of Figs. 6(b) and 6(c) finally allows to detect the increase of the remaining electrode deflection in comparison to the purely linear case.

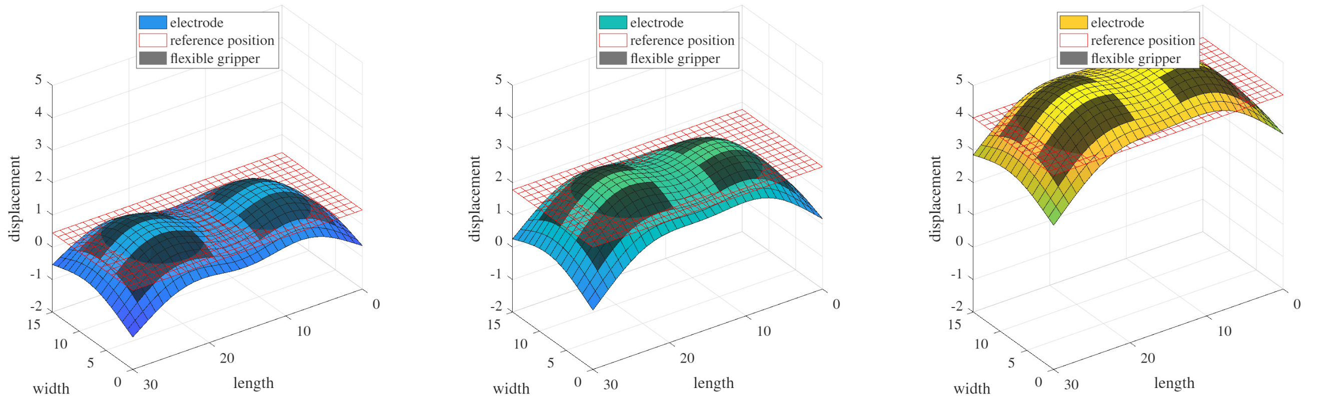

(a) Electrode deflection at $k = 200$.   (b) Electrode deflection at $k = 500$.   (c) Electrode deflection at $k = 2000$.

Fig. 5: Electrode deflection at different points in time in the PD controlled linear stacking process.

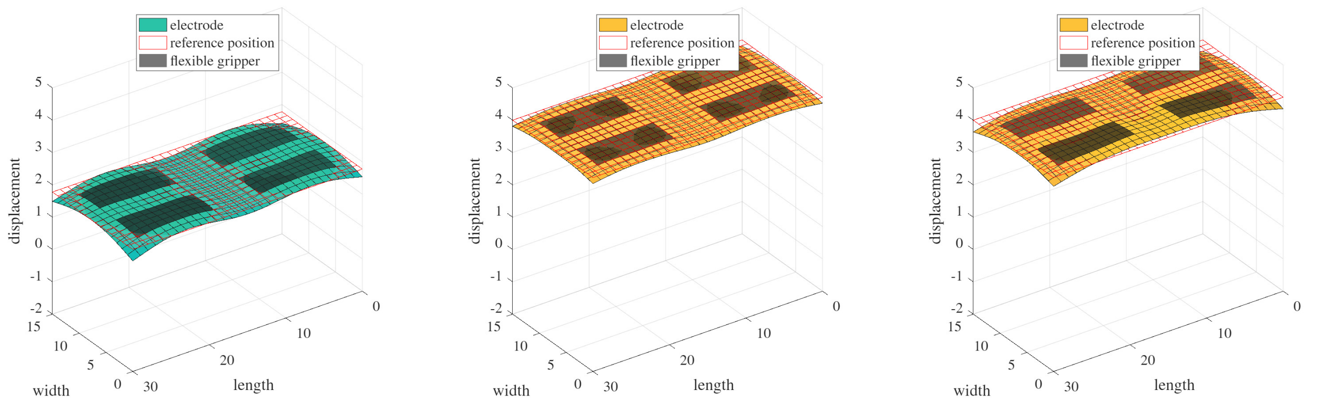

(a) Electrode deflection at $k = 500$ (linear).   (b) Electrode deflection at $k = 2000$ (linear).   (c) Electrode deflection at $k = 2000$ (nonlinear).

Fig. 6: Electrode deflection at different points in time in the PID controlled stacking process.

V. Conclusions and Outlook

In this paper, control-oriented modeling procedures have been derived for the representation of the mechanical deformation of electrodes during the battery production stages of notching and stacking.

In future work, these models will be extended to account for adhesion between two electrodes placed on top of each other when picking them up in stacking. Based on this extension, control approaches can be developed to overcome adhesion. Moreover, a further goal is the reduction of the deflection during stacking by means of state-feedback (instead of a heuristically tuned PD/PID) and by iterative learning control.

References

[1] B. Cichy, P. Augusta, K. Galkowski, A. Rauh, H. Aschemann, E. Rogers, and B. Rehak. Modeling and Iterative Learning Control of a Circular Deformable Mirror. *IFAC-PapersOnLine*, 50:3117–3122, 2017.

[2] B. Cichy, K. Galkowski, A. Rauh, H. Aschemann, and E. Rogers. A Practically Tractable Iterative Learning Control Scheme for a Circular Deformable Mirror. In *2017 10th International Workshop on Multidimensional (nD) Systems (nDS)*, pages 1–6, 2017.

[3] B. Cichy, K. Gałkowski, A. Rauh, and H. Aschemann. Iterative Learning Control of the Electrostatic Microbridge Actuator. In *2013 European Control Conference (ECC)*, pages 1192–1197, 2013.

[4] O. Demir, M. Colledani, G. Horváth, D. Marzogui, and K. Giakoumi. A Novel Zero-Defect Manufacturing Approach for Defect Reduction in Battery Production. *Procedia CIRP*, 134:1167–1172, 01 2025.

[5] B. Fornberg. Generation of Finite Difference Formulas on Arbitrarily Spaced Grids. 51(184):699–706, 1988.

[6] H. Heimes, A. Kampker, C. Offermanns, N. Lackner, T. Elliger, V. Mussehl, S. Michaelis, and J. Zienow. *Production of Lithium-Ion Battery Cell Components*. 2 edition, 2023.

[7] K. Husseini, N. Schmidgruber, H. Weinmann, K. Maibaum, J. Ruhland, and J. Fleischer. Development of a Digital Twin for Improved Ramp-Up Processes in the Context of Li-Ion-Battery-Cell-Stack-Formation. *Procedia CIRP*, 106:27–32, 2022. 9th CIRP Conference on Assembly Technology and Systems.

[8] S. Timoshenko and S. Woinowsky-Krieger. *The Theory of Plates and Shells*. Engineering Societies Monographs. McGraw-Hill, New York, USA, 2 edition, 1959.

[9] C. von Boeselager, M. O. Kapelar, and K. Dröder. Multi-Body Simulation of a Novel Electrode Stacking Process for Lithium-Ion Battery Production. *Procedia CIRP*, 112:519–524, 2022. 15th CIRP Conference on Intelligent Computation in Manufacturing Engineering.